Experimental and theoretical study about sulfur deactivation of Ni/CeO₂ and Rh/CeO₂ catalysts

Marco A. Ocsachoque [a, *], Juan I. Eugenio Russman [b], Beatriz Irigoyen [b], Delia Gazzoli [c], María G. González [a]

[a] Centro de Investigación y Desarrollo en Ciencias Aplicadas "Dr Jorge J. Ronco", (CONICET, CCT La Plata), Departamento de Química, Facultad de Cs Exactas (UNLP), Calle 48 N° 257, 1900 La Plata, Argentina
[b] Instituto de Tecnologías del Hidrógeno y Energías Sostenibles (ITHES), Departamento de Ingeniería Química, Facultad de Ingeniería (UBA), Buenos Aires, Argentina
[c] Dipartimento di Chimia, Universitá di Roma "La Sapienza", Roma, Italy

HIGHLIGHTS

- CeO₂ support can act as a sacrifice trap decreasing sulfur poisoning.
- Theoretical calculations indicate an important nickel affinity with sulfur.
- Rh would favor desorption of S–O species formed on the support.
- The O^{2-} species present on the Rh–CeO₂ sample favor sulfur removal.

ARTICLE INFO

ABSTRACT

Sulfur deactivation of Ni/CeO₂ and Rh/CeO₂ catalysts were examined through an experimental and theoretical study. These catalysts were characterized by N₂ adsorption, X-ray diffraction, temperature programmed reaction, thermogravimetric analysis, Uv–visible spectroscopy and Raman spectroscopy, and tested under the methane dry reforming reaction in the presence of H₂S. On the other hand, different possible interactions of sulfur with Rh, Ni or surface sites of the CeO₂ support were evaluated by performing energy calculations with the density functional theory (DFT). Overall, the results indicate that tolerance to sulfur of Rh/CeO₂ catalyst is higher than that of Ni/CeO₂ one. In this sense, TPR measurements show that reduction of CeO₂ is promoted by the presence of Rh. This effect, probably caused by hydrogen spillover to CeO₂ support during the reduction of RhOₓ species, could be linked to a high oxygen donation capacity of Rh/CeO₂ catalysts. Accordingly, the O^{2-} species existing on Rh/CeO₂ catalysts, revealed by Raman spectra of these samples, could favor sulfur oxidation and prevent Rh–S interactions. Likewise, the theoretical calculations show that desorption of S–O species from Rh/CeO₂ system is more favorable than that from Ni/CeO₂ one. Therefore, our experimental and theoretical study about sulfur deactivation of Ni and Rh supported on CeO₂ allow us to postulate that Rh can help to desorb SOₓ species formed on the support, retarding sulfur poisoning of the Rh/CeO₂ catalysts.

© 2016 Elsevier B.V. All rights reserved.

1. Introduction

The fact that sulfur compounds are present as usual impurities in sources to produce fuels and chemical products is widely well known [1,2]. In general, compounds as sulfides, mercaptans, thiophenes, benzothiophenes and dibenzothiophenes are found representing an important problem from industrial and environmental point of view [3–7]. When fuels are burnt, sulfur impurities react with the oxygen forming SOₓ-type sulfur oxides. These compounds can interact with water present in the atmosphere producing the so-called acid rain, that not only affects vegetation but also produces corrosion.

During hydrocarbon reforming reaction, sulfur compounds present in fuels are converted to SH₂ which can react on the

---

catalytic surface and adsorbs as atomic sulfur [8,9]. It is also well known that sulfur compounds are potent poisoning agents of the Ni-based catalysts used in methane reforming, as concentrations of 0.2 mg sulfur per m^2 of catalyst can lead to complete deactivation. Consequently, these poisoned catalysts lose the capacity to reform hydrocarbons, producing their pyrolysis [10]. Other studies have indicated that the activity of Ni-based catalysts may be improved by adding noble metals to the Ni active phase as well as promoting the support with CeO_2 [11–16]. However, relatively little attention has been directed to sulfur effects on the methane reaction with CO_2, despite the fact that both natural gas and biogas have appreciably amounts of sulfur-containing species.

The poisoning process in metallic catalysts can be schematized through the following reaction:

$$H_2S + Me \leftrightarrow Me - S + H_2 \qquad (1)$$

Several researchers have stated that sulfur is joined to the metallic site forming stable compounds with transition metals [8], and leading to catalyst poisoning by sulfur deposition. In this sense, it is well known that nickel is one of the most sensitive metals to this poisoning.

On the other hand, different works have indicated that CeO_2 [15] provides labile oxygen anions that can oxidize the S-containing species formed from H_2S and, thus, favor their removal in the form of SO_2. In a previous study about Rh/α-Al_2O_3–CeO_2 catalysts [16], we showed that CeO_2 has an important role in preventing sulfur poisoning of these samples during methane dry reforming process. Therefore, in the present study we employed experimental characterization techniques together with theoretical DFT calculations for examining sulfur effects on both Rh and Ni active phases supported on CeO_2. In this sense, our results can provide some useful keys for the development of solids with high resistance to sulfur poisoning; which, in turn, would be adequate catalysts for the methane dry reforming process.

2. Experimental

2.1. Catalysts preparation

The CeO_2 support was prepared from commercial salt $(NH_4)_2[Ce(NO_3)_6]$ calcined at 650 °C for 4 h. Monometallic catalysts containing 5% Rh wt/wt and 5% Ni wt/wt were prepared by incipient wetness impregnation with aqueous solutions of Cl_3Rh and $Ni(NO_3)_2$. For Rh-based catalyst, the support was impregnated with Rh salt and calcined at 350 °C for 1 h; while for the another monometallic catalyst, Ni salt was added to the support and calcined at 500 °C for 1 h. Finally, under this methodology, the following catalysts were obtained: Rh(5%)/CeO_2 and Ni(5%)/CeO_2.

2.2. Characterization of catalysts

The catalysts were characterized by N_2 adsorption-BET analysis, X-ray diffraction (XRD), temperature programmed reaction (TPR), thermogravimetric analysis (TGA), Uv–visible spectroscopy (UV–Vis), diffuse reflectance spectroscopy (DRS) and Raman spectroscopy. Physicochemical properties effect on catalysts behavior were also analyzed with special emphasis in deactivation problems. BET surface area and pore volume distributions were measured by N_2 adsorption at −196 °C, in a Micromeritics Accusorb 2100E analyzer. The samples were outgassed at 100 °C, for 12 h, before adsorption.

The phases present in the catalysts were identified by X-ray diffraction analysis. For this, we used a Philips PW 1740 equipment with Cu Kα radiation, under 20 mA current and 40 kV voltage, with a scanning rate of 2I/min, and an interval for the analysis from 5 to 70I.

The reducibility of the samples was determined in a conventional TPR equipment. A 0.1 g of sample was loaded in a quartz reactor and heated from room temperature to 900IC, at a rate of 10IC/min, under 10% (v/v) H_2/N_2 stream with a gas flow rate of 20 cm^3 min^{-1}. The response was measured with a thermal conductivity detector.

Diffuse reflectance spectra were obtained with spectrophotometer Varian UV–visible, with diffuse reflectance chamber with integrating sphere. The range used for these measurements was 200–800 nm.

The Raman spectrum was collected on powder samples at room temperature by means of a Via Renishaw spectrometer, equipped with CCD detector and super Notch filter, using the line 488.0 nm of an Ar$^+$ laser.

2.3. Catalytic activity

Catalytic properties of the samples were determined in a flow system through a fixed bed quartz reactor with 9 mm internal diameter connected in line to a Perkin Elmer chromatograph with thermal conductivity detector. The catalysts were previously reduced in H_2 stream for 1 h at 650 °C; the mass catalyst used was 30 mg. The reactor was fed at a flow rate of 102 cm^3 min^{-1} (CH_4/CO_2/He/H_2 = 6/14/66/15 cm^3 min^{-1}, CH_4/CO_2: 0.5).

After catalysts reduction, the samples were tested for methane dry reforming reactions at 650 °C and atmospheric pressure, under chemical control conditions. In this regard, the catalysts were first evaluated in an environment free of sulfur until a constant activity was reached. Then, the catalysts sulfur deactivation was studied by adding 0.02 ppm of H_2S to the reactor feed. These reactions were evaluated until the catalyst activity decreased to zero.

3. Computational

3.1. Catalysts models

Cerium oxide (CeO_2) has a fluorite structure (CaF_2) consisting of a cubic close-packed array of Ce cations with all tetrahedral holes filled by O anions. The reported experimental value of the CeO_2 lattice parameter is 5.41 Å [17], while we calculated a theoretical value of 5.49 Å. Concerning the catalytic surface, we employed the (111) plane. This face is one of the most stable among those of low index, and corresponds to the minimal Ce–O bonds cleavage [18–20]. Thus, the $CeO_2(111)$ surface was terminated with an extra oxygen plane and modeled with a slab formed by 12 atomic (Ce and O) layers and a vacuum space of about 12 Å, which was introduced to avoid interactions between periodic images. The positions of adsorbates and those of Ce and O ions on top layers were fully optimized, until reaching a convergence value of 0.02 eV/Å for the forces acting on atoms. Ce and O ions located on bottom layers were kept fix as to mimic the bulk solid.

3.2. DFT calculations

In this work, we performed energy calculations applying the density functional theory (DFT) as implemented in the Vienna Ab-initio Simulation Package [21,22]. The Kohn–Sham equations were solved with the generalized gradient approximation (GGA) and the Perdew–Burke–Ernzerhof (PBE) exchange-correlation functional [23]. The core electrons were represented with the projector augmented wave (PAW) method [24,25]. For valence electrons we used the configurations Ce ($5s^2$, $5p^6$, $6s^2$, $5d^1$,$4f^1$) and O ($2s^2$, $2p^4$). The wave functions were expanded using a truncation energy value

of 410 eV, and the tolerance for the total free energy change was set in 10^{-4} eV. The Brillouin zone was sampled with a $4 \times 4 \times 1$ k-points grid according to the Monkhorst–Pack scheme [26], and we used a Gaussian smearing of 0.2 eV. For all energy calculations we considered spin polarization effects.

The standard DFT formulation usually fails to describe strongly correlated electrons due to a deficient treatment of electron correlation. This limitation was corrected by using the DFT + U method, where the introduction of a Hubbard parameter U modified the self-interaction error and enhanced the description of the correlation effects [27,28]. We used a Hubbard parameter U = 5 eV to describe the on-site Coulomb interaction of the Ce(4f) electrons. This value is consistent with the recommendations of Nolan et al., who reported that CeO_2 structure essentially converges with respect to localization for a value of the U parameter greater or equal to 5.0 eV [29,30].

Rh and nickel (Me) atoms adsorption energy was calculated as the difference between the total free energy of the $Me/CeO_2(111)$ system, and those of the bare $CeO_2(111)$ surface terminated with an extra layer of oxygen atoms and the Ni or Rh atom:

$$\Delta E_{ads,Me} = E[Me/CeO_2(111)] - E[CeO_2(111)] - E[Me].$$

In this equation, Me indicates Rh or Ni. A negative value of $\Delta E_{ads,Me}$ means that Ni or Rh interaction on surface sites is stable. The energy value of atomic nickel was taken as the lowest triplet state, Ni (d9, s1): E[Ni] = −0.52 eV [31].

Then, sulfur adsorption energy on $Me/CeO_2(111)$ surface was calculated as:

$$\Delta E_{ads,S} = E[S-Me/CeO_2(111)] - E[Me/CeO_2(111)] - E[S]$$

where E [S] is the total energy of a S atom in vacuum.

4. Results and discussion

4.1. Morphological characteristics of catalysts

$Ni(5\%)/CeO_2$ and $Rh(5\%)/CeO_2$ samples were characterized with the N_2 adsorption technique, while experimental data were fitted by applying the BET theory. The results are shown in Table 1.

It is possible to observe that textural parameters of catalysts are defined by the CeO_2 support utilized as reference. Moreover, the addition of metals does not produce significant changes in the specific surface of the studied samples. However, Ni addition to CeO_2 support led to an increase in the average pore volume of this catalyst. This effect would be related to Ni particles blockage of the support narrow pores [32]. This fact does not occur for the $Rh(5\%)/CeO_2$ catalyst, suggesting that Rh particles are smaller than the Ni ones.

4.2. X-ray diffraction

Fig. 1, presents X-ray diffraction patterns that were used to identify different species through analysis of peaks characteristic of the support as well as the active phases.

Table 1
Morphological properties.

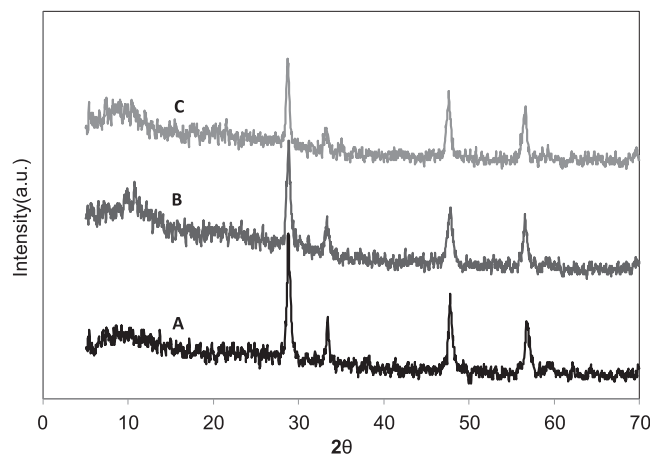| Catalyst	Sg (m²/g)	Average Vp (m³/g)
CeO_2	19	0.062
$Ni(5\%)/CeO_2$	18	0.094
$Rh(5\%)/CeO_2$	17	0.069

Fig. 1. XRD patterns of the reduced fresh catalysts. References: (A) CeO_2, (B) $Ni(5\%)/CeO_2$, (C) $Rh(5\%)/CeO_2$.

Signals around $\theta = 44.5$ and $51.9°$ (JCPDS 87-0712) correspond with the presence of Ni°. The CeO_2 is evidenced by the signals at $\theta = 28$, 33, 47 and 56° (JCPDS-4-0593). The CeO_2 support has a face center cubic of fluorite-type crystalline structure. The signal at $\theta = 47°$, associated to Rh° (JCPDS-4-0593), overlaps with that of CeO_2.

4.3. Temperature programmed reduction

Fig. 2, shows the temperature programmed reduction (TPR) profiles of bare CeO_2 support and catalysts. The profile for support (Fig. 2A) shows CeO_2 reduction peaks at 512 °C, with hydrogen consumption starting from 804 °C. The first peak would correspond to surface oxygen species, while the signal at high temperature can be associated to CeO_2 total reduction by removal of oxide ions from the bulk lattice. The peak at low temperature can be attributed to surface oxygen ions, while the one at high temperature is assigned to reduction of Ce^{4+} to Ce^{3+}. Therefore, reduction at high temperatures can lead to non stoichiometric oxides with oxygen deficiency of CeO_x (1.714 < x < 2) composition.

As it can be seen in Fig. 2, the $Rh(5\%)/CeO_2$ catalyst presents reduction signals at 130 °C and 290 °C. The first one is associated to reduction of free Rh_2O_3, while the second peak corresponds to that
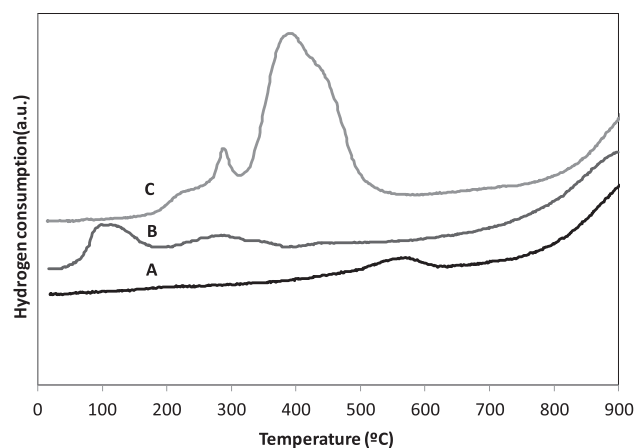

Fig. 2. TPR profiles of the different catalysts. References: (A) CeO_2, (B) $Rh(5\%)/CeO_2$, (C) $Ni(5\%)/CeO_2$.

of Rh_2O_3 interacting with CeO_2 support.

Comparison of reduction profiles of Rh(5%)/CeO_2 and CeO_2 catalysts indicates that the presence of Rh promotes CeO_2 reduction, which can be attributed to hydrogen spillover during RhO_x reduction [12]. Similar phenomena were observed for Rh and Ni—Rh supported on CeO_2—Al_2O_3 [12,14]. On the other hand, Ni(5%)/CeO_2 catalyst presents H_2 consumptions at 235, 290 and 400 °C; these peaks would be associated to reduction of NiO particles dispersed on the CeO_2 matrix. Finally, it is worthy to note that both catalysts show hydrogen consumption at 800 °C in association with reduction of the CeO_2 support.

Previous XPS studies on Ni—Rh/CeO_2—AlO_2 catalysts, tested in the same conditions than used in this work, have shown two peaks in Rh 3d region which were adjudicated to the coexistence of Rh° and Rh^+ species [14]. Wang et al. [33], attributed this fact to an interaction between Rh and CeO_2, which is in agreement with TPR data. The presence of Rh^+ species in CeO_2‑containing catalysts can be associated to the redox cerium (Ce^{3+}/Ce^{4+}) properties. The Ce 3d region presents Ce^{3+} and Ce^{4+} contributions, indicating that Rh presence favors Ce reduction. Therefore, activation of CH_4 can be promoted by partially oxidized Rh^+ species due to a fast recovery of their metallic state, which is a fundamental condition for improving the catalytic activity.

Uv—visible spectra of the studied samples (not shown here) present an absorption band below 400 nm, which corresponds to the CeO_2 support. The band attributed to charge transfer from O^{2-} to Ce^{4+} appears at 278 nm and that to Ce^{3+} is near to 255 nm [34].

4.4. Raman spectroscopy

Raman spectroscopy was used to analyze the catalysts and visualize the presence of sulfur compounds able to cause their deactivation. Fig. 3, shows the Raman spectra obtained for both samples, before and after reaction.

The spectrum of fresh Rh/CeO_2 catalyst reduced in H_2 at 650 °C and exposed to atmosphere (Fig. 3A), presents bands around 455,

572, 1165 cm^{-1} [35—37]. The most intense band is attributed to the vibration mode (F_{2g}) of CeO_2 with a fluorite-type cubic structure, while the weakest band at 572 cm^{-1} is due to defect-induced mode (D) for oxygen vacancies in the ceria structure. In the deactivated Rh/CeO_2 sample (Fig. 3b), the band near 570 cm^{-1} presents lower intensity than in the reduced sample; while the ratio between bands at 1160 and 455 cm^{-1} does not change appreciably. This indicates that the redox process occurs on the surface. Particularly, the band around 1100 cm^{-1} is associated to sulfate species [38—40].

In the Ni(5%)/CeO_2 sample (Fig. 3c), reduced at 650 °C and exposed to the atmosphere, the spectrum shows bands at 457, 570 and 1170 cm^{-1}. The most intense band corresponds to the CeO_2 fluorite structure, whereas the band at 570 cm^{-1} corresponds to oxygen vacancies in the CeO_2 lattice. Bands corresponding to NiO species are not observed [41,42].

The spectrum of Ni samples extracted from the reactor (Fig. 3d) shows particles of CeO_2, and of both CeO_2 and carbon. Bands at 453, 575 and 1170 cm^{-1} are attributed to CeO_2, while the band at 1010 cm^{-1} is ascribed to sulfate species. The D band at low frequency is attributed to defects that involve O^{2-} vacancies, while the presence of this band at high frequencies could be produced by the inclusion of dopants. The band near 610 cm^{-1} may contain contributions of sulfate groups adsorbed on the catalyst surface. Note that bands at 1350 and 1580 cm^{-1}, which would be associated to the presence of carbon [43], are not observed for Rh(5%)/CeO_2 catalyst. These results indicate that both samples were deactivated by the sulfur present in the feed. Furthermore, the bands at 1350 and 1580 cm^{-1} observed in the Ni(5%)/CeO_2 used sample spectrum can be associated to the presence of filamentous carbon species. The wide band in the range 1010—1080 cm^{-1} is ascribed to stretching and anti-stretching modes of sulfate species.

4.5. Theoretical characterization of Rh/CeO_2(111) and Ni/CeO_2(111) solids

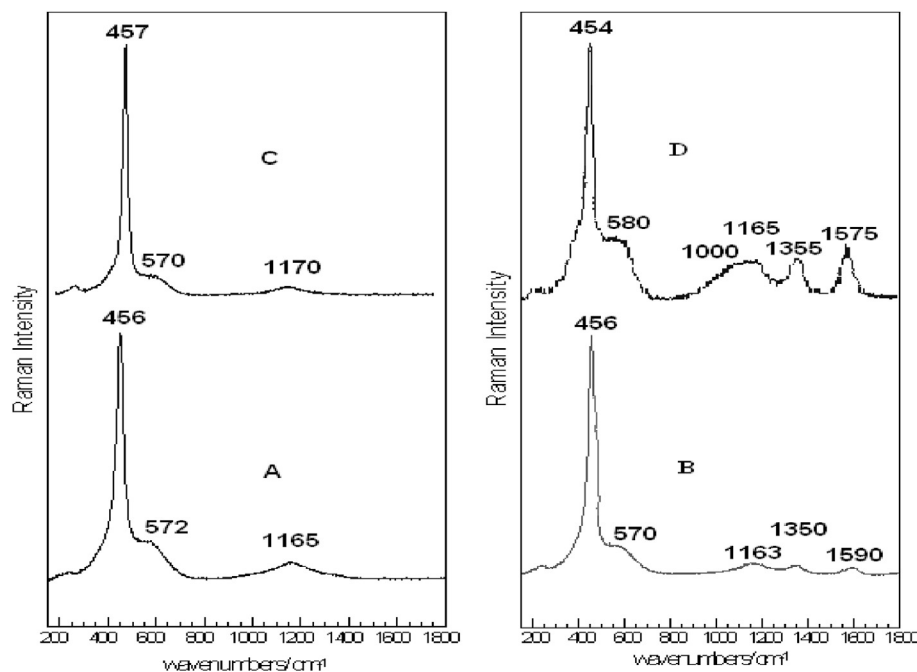CeO_2(111) surface exhibits different sites to study adsorbate

Fig. 3. Raman spectra of Rh(5%)CeO_2 and Ni(5%)CeO_2 catalysts, before after dry reforming reaction. References: (A) Rh(5%)CeO_2 treated in H_2 at 650 °C; (B) Rh(5%)CeO_2 after catalytic test; (C) Ni(5%)/CeO_2 treated in H_2 at 650 °C; (D) Ni(5%)/CeO_2 after catalytic test.

interactions: Ce cations, surface and subsurface O anions, and positions between O anions, and Ce and O ions. Oxygen anions located on the O-uppermost layer were identified as O_u, and those located on the O-subsurface layer as O_d. The position between surface oxygen anions was identified as O–O bridge, while that between surface cerium and oxygen as Ce–O bridge. The calculated energy values for Rh adsorptions on Ce, O_u and O_d sites are reported in Table 2.

The evaluation of Rh interactions over O–O and Ce–O bridge positions indicates that these systems would relax into one of the aforementioned structures. The most favorable of those interactions corresponds to Rh located over a subsurface oxygen (O_d) with a calculated adsorption energy value of −2.53 eV, where Rh is surrounded by three surface oxygen anions. These anions displaced 0.23 Å toward Rh (Fig. 4), resulting in Rh–O distances of 2.18 Å. Our calculations also show that Rh could form adsorbed cluster-type structures. The computed Rh_4-cluster interactions ($\Delta E_{ads,Rh} = -3.56$ eV/Rh atom) indicate the Rh_4–$CeO_2(111)$ system is stabilized by additional 1.04 eV/Rh atom.

On the other hand, Ni deposition on $CeO_2(111)$ surface was studied by calculating Ni adsorption energy on Ce, O_u, O_d and O–O bridge sites. The energy value corresponding to Ni located at Ce–O bridge could not be evaluated because Ni relaxed to a position over the O–O bridge site. The calculated adsorption energy for Ni interaction on Ce site is $\Delta E_{ads,Ni} = -1.28$ eV (Table 3). Due to this interaction, Ni located at 2.24 Å of Ce; which descended 0.11 Å into the bulk, reflecting some Ni–Ce repulsive effect.

Ni interactions on surface oxygen (O_u site) resulted in $\Delta E_{ads,Ni} = -2.31$ eV. Ni located at 1.74 Å of that oxygen, which moved 0.13 Å out of the surface. Consequently, its Ce–O bonds length increased up to 2.46 Å. Ni deposition on the subsurface O_d site is 0.51 eV more favorable than that on the O_u one (Table 3). The atomic structure optimization shows that Ni was located in the center of a triangle formed by three surface O anions (d(Ni–O) = 2.0 Å). These oxygen ions raised 0.31 Å and also moved on the plane, increasing their Ce–O bonds distance up to 2.79 Å.

The most favorable Ni interaction on $CeO_2(111)$ surface resulted from Ni adsorption on the O–O bridge position ($\Delta E_{ads,Ni} = -3.36$ eV). The optimized atomic structure is shown in Fig. 5. As it can be seen, Ni located at 1.86 Å of each of the O anions; which positions were relaxed on the plane (0.33 Å and 0.36 Å, respectively) and also moved 0.40 Å out of the surface. Meanwhile, the corresponding Ce–O distances were enlarged up to 0.45 Å.

4.6. Catalytic tests

All catalysts were tested in methane dry reforming reactions and their resistance to sulfur poisoning was studied by adding 0.02 ppm of H_2S to the reactor feed. Fig. 6, presents normalized activity (reaction rate at time t/reaction rate at t = 0) as function of reaction time for methane dry reforming at 650 °C on Rh and Ni samples supported on CeO_2. For comparison, the behavior of these samples supported on CeO_2–Al_2O_3 was also studied.

Fig. 6, shows that all catalysts present a marked fall of their activity; which finally leads to the total activity loss. In reaction, the Ni(5%)/CeO_2 catalyst deactivates completely at 200 min. On the
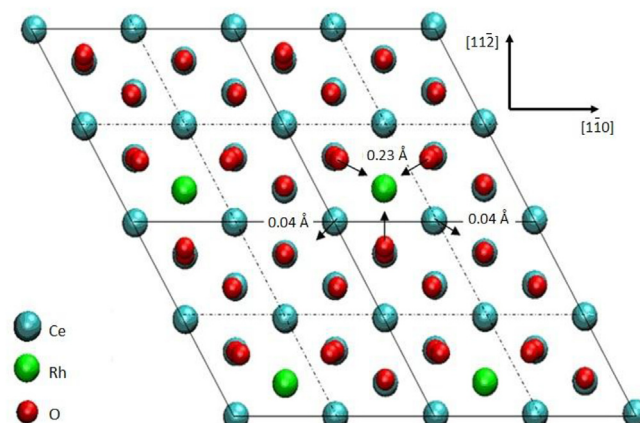

Fig. 4. Rh adsorption on the $CeO_2(111)$ surface.

Table 3
Adsorption energy values for Ni interactions on the $CeO_2(111)$ surface.

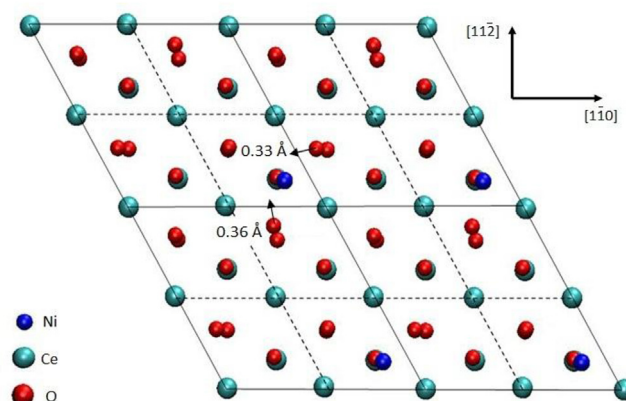| Site	Energy (eV)
Ce	−1.28
O_u	−2.31
O_d	−2.82
O–O bridge	−3.36

Fig. 5. Ni adsorption on the O–O bridge position on the $CeO_2(111)$ surface.
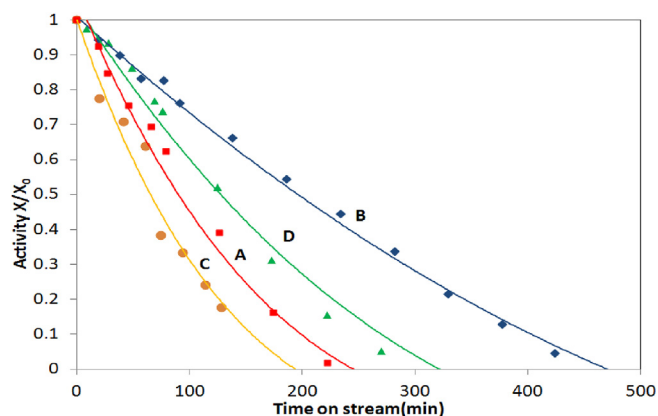

Fig. 6. Catalysts normalized activity in the presence of 0.02 ppm of H_2S. References: (A) Ni(5%)/CeO_2, (B) Rh(5%)//CeO_2,(C) Ni/$CeAl_2O_3$, (D) Ni–Rh/CeO_2–Al_2O_3.

Table 2
Adsorption energy values for Rh interactions on the $CeO_2(111)$ surface.

Site	Energy (eV)
O_d	−2.52
O_u	−1.84
Ce	−1.64

other hand, the Rh(5%)/CeO$_2$ catalyst shows a remainder activity equal to 0.45 of the initial activity, in the same time. Herewith, the Rh(5%)/CeO$_2$ catalyst requests longer reaction times to achieve the same activity than mono and bimetallic Ni-containing catalysts; thus, revealing that the Rh sample has higher tolerance to sulfur poisoning than the Ni one. These results are in good agreement with reports of bibliography; which indicates that, at similar operation conditions, Ni is more sensitive to sulfur deactivation than noble metals in the methane dry reforming process [7,13,15]. On the other hand, the curves depicted in the Fig. 6 show an almost linear relationship between activity and time reaction, which suggests that deactivation of catalysts occurs at constant reaction rate. This fact indicates that this process would be represented by first order deactivation kinetics.

As previously discussed, sulfonates and sulfates species would predominate in the Rh(5%)/CeO$_2$ catalyst; these species can prevent Rh–S interactions, determining the better performance of Rh(5%)/ CeO$_2$ catalyst.

Previous experiments have demonstrated that the bimetallic Ni–Rh/CeO$_2$–Al$_2$O$_3$ catalyst presents an increased activity in methane dry reforming with respect to that of the monometallic Ni one [14], evidencing the positive effect of Rh and CeO$_2$ combined presence in improving the thioresistance. Moreover, the characterization results indicate a synergetic interaction between Rh and CeO$_2$ support. In this sense, the Rh/CeO$_2$ group would operate as an active site for methane reforming with CO$_2$; causing the activation of methane on Rh sites, while that of CO$_2$ on the CeO$_2$ support. In the bimetallic catalysts, according to Yi et al. [12], the active sites are formed by Rh–Ni–Ce particles and the hydrocarbon would be activated on the Ni–Rh sites.

4.7. DFT calculations

Sulfur interactions on Ce, O$_u$, O$_d$ and Ce–O bridge sites of clean CeO$_2$(111) surface were evaluated in a previous work [44]. The most exothermic interaction corresponded to a S atom located over the Ce–O bridge site, with a S adsorption energy value of −2.38 eV. Sulfur deposition over the Ce–O bridge site resulted in S–O and S–Ce bonds length of 1.70 Å and 2.78 Å, respectively. Due to this interaction, the O was moved 0.18 Å out of the surface, approximating to S and increasing the corresponding Ce–O distance in 0.26 Å.

Besides, sulfur interactions were evaluated on different sites of the Rh$_{(Od)}$-CeO$_2$(111) surface because of Rh preferential adsorption over subsurface oxygen O$_d$ [43]. The adsorption energy values were calculated for S interactions on-top of Ce and Rh cations, on surface O$_u$ and subsurface O$_d$ oxygen anions and also over O–O and Ce–O bridge positions. The most favorable of those sulfur interactions (Table 4) corresponds to a S atom deposited on surface O coordinated to Rh ($\Delta_{Eads,S-Ou} = -3.73$ eV). This oxygen bonded to S atom after being moved 0.58 Å away from Rh, and 0.47 Å above the surface. Rh atomic position was also relaxed 0.20 Å out of the surface and 0.33 Å on the plane.

It is worthy to note that S atom adsorption on-top of oxygen O$_u$

on the Rh$_{(Od)}$/CeO$_2$(111) system was 1.35 eV more favorable than that on the CeO$_2$(111) one. This reflected in the length of the S–O bond, which is 0.07 Å shorter than that measured on CeO$_2$(111) surface (1.63 vs. 1.70 Å, respectively). Moreover, sulfur adsorption on Rh ($\Delta_{Eads,S-Rh} = -3.38$ eV) was 0.35 eV less favorable than that on surface oxygen O$_u$. Due to this interaction, Rh was moved 0.29 Å out of the surface forming a Rh–S bond of 2.09 Å length.

Regarding the present work, sulfur interactions on Ni/CeO$_2$(111) system were evaluated by considering the configuration resulting from Ni preferential adsorption between two surface oxygen (the O–O bridge position). The calculated adsorption energy values for S interaction on different Ni$_{(O-O)}$/CeO$_2$(111) surface sites are reported in Table 5.

When S atom was located on a subsurface oxygen (O$_d$ site) or Ce cations, it relaxed on-top of surface oxygen anions. Thus, in order to evaluated these interactions we allowed S to relax only in the (111) direction (z-coordinate). We calculated adsorption energy values for the optimized S–O$_d$ and S–Ce structures of −1.81 and −2.52 eV, respectively. Sulfur deposition on Ni resulted in an adsorption energy value of $\Delta_{Eads,S} = -3.26$ eV. The S atom located at 2.0 Å distance of Ni, forming stable S–Ni species. This is an indication of the important sulfur affinity with nickel.

The most exothermic sulfur interaction resulted from S atom deposition on-top of a surface oxygen O$_u$ coordinated to Ni ($\Delta_{Eads,S} = -3.54$ eV), and it is 0.28 eV more favorable than that on Ni. Sulfur bonded to this oxygen forming a S–O bond of 1.70 Å length, similar to that resulting from S deposition on clean CeO$_2$(111) surface. The oxygen position was stretched 0.48 Å on the plane (Fig. 7), increasing the O–Ni distance in 1.05 Å. Consequently, Ni was moved 0.84 Å to another surface O and pushed it by 0.47 Å.

The previous findings suggest that S adsorption on-top of oxygen anions of Rh–CeO$_2$ interface weakened the corresponding O–Ce bonds and, thus, could promote the desorption of the formed S–O species. Therefore, we evaluated the energetics of that process for S–Ni$_{(O-O)}$/CeO$_2$(111) and S–Rh$_{(Od)}$/CeO$_2$(111) systems.

The S–O species desorption energy was calculated as:

$$\Delta E_{desorc,\ S-O} = E\ [Me/CeO_2{}^*] + E\ [S-O] - E\ [S-Me/CeO_2]$$

In this equation, Me indicates Rh or Ni; while Me/CeO$_2$* represents the resulting Ni$_{(O-O)}$/CeO$_2$(111) or Rh$_{(Od)}$/CeO$_2$(111) system with a surface oxygen vacancy.

The computed energy values show that S–O species desorption from both catalysts, Rh or Ni supported on CeO$_2$, are endothermic processes. The calculations show that removal of S–O species from the Rh$_{(Od)}$/CeO$_2$(111) surface (3.62 eV) is 1.97 eV easier than that from the Ni$_{(O-O)}$/CeO$_2$(111) one. However, the formation of a surface oxygen vacancy on these catalysts was computed in about 3.2 eV. These results would suggest that Rh promotes desorption of S–O compounds from Rh/CeO$_2$ interface.

On the whole, the theoretical calculations indicate that CeO$_2$ support could mitigate sulfur poisoning and deactivation of Me active phases by promoting the formation of oxidized sulfur compounds. Meanwhile, Rh would favor the easy desorption of these compounds from the CeO$_2$ support. These indications are in good

Table 4
Adsorption energy values for S atom interactions on the Rh$_{(Od)}$/CeO$_2$(111) surface.

Site	Energy (eV)
O$_d$	−1.05
Ce–O	−2.50
Ce	−2.75
Rh	−3.38
O$_u$	−3.73

Table 5
Adsorption energy values for S atom interactions on the Ni$_{(O-O)}$/CeO$_2$(111) surface.

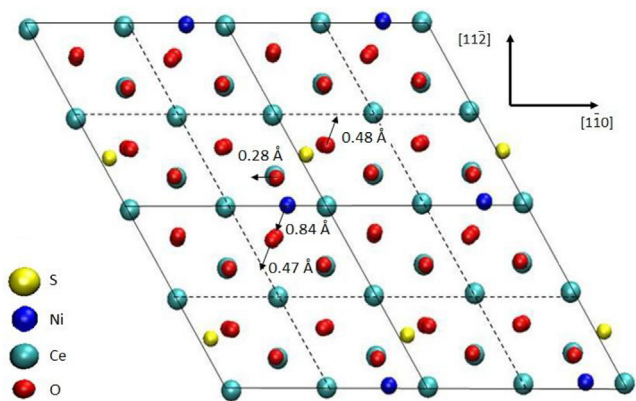| Site	Energy (eV)
O$_d$	−1.81
Ce	−2.52
Ni	−3.26
O$_u$	−3.54

Fig. 7. Sulfur adsorption on oxygen site O_u on the $Ni_{(O-O)}/CeO_2(111)$ surface.

agreement with experimental findings suggesting that CeO_2 promotes the effective sulfur oxidation on CeO_2/Al_2O_3 supports, while Rh facilitates the migration of oxidized sulfur species.

The experimental and theoretical results exposed in this work are in agreement with previous reports which indicate that Ni, when located close to Rh, can protect Rh from sulfur poisoning [11]. The catalytic behavior of $Ni/CeO_2-Al_2O_3$ and $Rh/CeO_2-Al_2O_3$ suggests that addition of CeO_2 to alumina enhances the sulfur poisoning resistance. This fact would be attributed to the presence of labile oxygen anions, provided by CeO_2, that can oxidize the S-containing species to SO_2 which left the catalyst more easily. In this sense, it has been reported that the presence of O^{2-} anions favors the removal of S-containing species as SO_2. Karjalainen et al. [45], demonstrated by means of thermodynamic calculations that CeO_2 acts as sulfur adsorbent in a reducing atmosphere, forming compounds such as $Ce(SO_2)_3$ and Ce_2O_2S. These authors also stated that sulfur adsorption is not altered by the presence of noble metals since S interaction with CeO_2 is thermodynamically more favorable than that with noble metals. In this way, the adsorbent capacity of CeO_2 can regulate the catalyst useful life and, thus, the activity would fall down to zero after occupation of all adsorption sites [44]. These results can explain the increased thioresistance observed when Rh and CeO_2 are added together as promoters of Ni/Al_2O_3 catalysts. Similarly, the addition of CeO_2 to Rh/Al_2O_3 catalysts also results in a higher resistance to poisoning by sulfur, although in both cases a total deactivation is reached [11].

5. Conclusions

In this work, we employed diverse experimental techniques as well as DFT calculations to fully understand the influence of metallic phases (Ni,Rh) and CeO_2 support on the sulfur deactivation of Rh/CeO_2 and Ni/CeO_2 catalysts during methane dry reforming.

The evaluation of these catalysts demonstrated that Rh/CeO_2 presents higher tolerance to sulfur than Ni/CeO_2. Theoretical calculations showed that desorption of S—O species from Rh/CeO_2 is more favorable than that from $Ni—CeO_2$, in agreement with the experimental findings of this work. As regard, the O^{2-} species present on the $Rh—CeO_2$ sample, determined by Raman spectroscopy, favors sulfur removal in the form of SO_2 species and prevents Rh—S interactions.

In summary, our experimental and theoretical results indicate that the CeO_2 support could act as a sacrifice trap decreasing sulfur poisoning and deactivation of Rh metallic phase. Likewise, Rh would favor desorption of S—O species formed on that support retarding the poisoning by sulfur of Rh/CeO_2 catalyst.

References

[1] H. Topsoe, B.S. Clausen, F.E. Massoth, Hydrotreating Catalysis: Science and Technology, Springer, Heidelberg, 1996.

[2] J.G. Speight, The Chemistry and Technology of Petroleum, second ed., Dekker, New York, 1991.

[3] A.C. Stern, R.W. Boubel, D.B. Turner, D.L. Fox, Fundamentals of Air Pollution, second ed., Academic Press, Orlando, 1984.

[4] K.C. Taylor, Nitric oxide catalysis in automotive exhaust systems, Catal. Rev. Sci. Eng. 35 (1993) 457—481.

[5] J.M. Thomas, W.J. Thomas, Principles and Practice of Heterogeneous Catalysis, VCH, New York, 1997.

[6] B.C. Gates, Catalytic Chemistry, Wiley, New York, 1992.

[7] C.H. Bartholomew, P.K. Agrawal, J.R. Katzer, Sulfur poisoning of metals, Adv. Catal. 31 (1982) 135—242.

[8] J. Sehested, Four challenges for nickel steam-reforming catalysts, Catal. Today 111 (2006) 103.

[9] Y. Chen, C. Xie, Y. Li, C. Song, T.B. Bolin, Sulfur poisoning mechanism of steam reforming catalysts: an x-ray absorption near edge structure (XANES) spectroscopic study, Phys. Chem. Chem. Phys. 12 (2010) 5707—5711.

[10] J.R. Rostrup- Nielsen, Conversion of hydrocarbons and alcohols for fuel cells, Phys. Chem. Chem. Phys. 3 (2001) 283—288.

[11] J.J. Strohm, J. Zheng, C. Song, Low-temperature steam reforming of jet fuel in the absence and presence of sulfur over Rh and Rh—Ni catalysts for fuel cells, J. Catal. 238 (2006) 309—320.

[12] Y. Li, X. Wang, C. Xie, C. Song, Influence of ceria and nickel addition to alumina-supported Rh catalyst for propane steam reforming at low temperatures, Appl. Catal. A 357 (2009) 213—222.

[13] C. Xie, Y. Chen, Y. Li, X. Wang, C. Song, Sulfur poisoning of $CeO_2-Al_2O_3$-supported mono- and bi-metallic Ni and Rh catalysts in steam reforming of liquid hydrocarbons at low and high temperatures, Appl. Catal. A 390 (2010) 210—218.

[14] M. Ocsachoque, F. Pompeo, G. González, Rh—$Ni/CeO_2-Al_2O_3$ catalysts for methane dry reforming, Catal. Today 172 (2011) 226—231.

[15] A. Erdohelyi, K. Fodor, T. Szailer, Effect of H_2S on the reaction of methane with carbon dioxide over supported Rh catalysts, Appl. Catal. B Environ. 53 (2004) 153—160.

[16] M. Ocsachoque, J. Bengoa, D. Gazzoli, M.G. González, Role of CeO_2 in Rh/α-Al_2O_3 catalysts for CO_2 reforming of methane, Catal. Lett. 141 (2011) 1643—1650.

[17] L. Eyring, in: K.A. Gschneider, L. Eyring (Eds.), Handbook on the Physics and Chemistry of Rare Earths, 1979. Amsterdam.

[18] J.C. Conesa, Computer modeling of surfaces and defects on cerium dioxide, Surf. Sci. 339 (1995) 337—352.

[19] M. Nolan, S. Grigoleit, D.C. Sayle, S.C. Parker, G.W. Watson, Density functional theory studies of the structure and electronic structure of pure and defective low index surfaces of ceria, Surf. Sci. 576 (2005) 217—229.

[20] N.V. Skorodumova, M. Baudin, K. Hermansson, Surface properties of CeO_2 from first principles, Phys. Rev. B 69 (7) (2004) 075401 (1—8).

[21] G. Kresse, J. Furthmuller, Efficiency of ab-initio total energy calculations for metals and semiconductors using a plane-wave basis set, Comput. Mater. Sci. 6 (1996) 15—50.

[22] G. Kesse, J. Hafner, Ab initio molecular dynamics for liquid metals, Phys. Rev. B Cond. Matter Mater. Phys. 47 (1993) 558—561.

[23] J.P. Perdew, K. Burke, M. Ernzerhof, Generalized gradient approximation made simple, Phys. Rev. Lett. 77 (1996) 3865—3871.

[24] G. Kresse, D. Joubert, From ultrasoft pseudopotentials to the projector augmented-wave method, Phys. Rev. B Cond. Matter Mater. Phys. 59 (1999) 1758—1775.

[25] P.E. Blöchl, Projector augmented-wave method, Phys. Rev. B Cond. Matter Mater. Phys. 50 (1994) 17953—17979.

[26] H.J. Monkhorst, J.D. Pack, Study of the ω phase in Zr—Nb alloys by Mössbauer and X-ray diffuse scattering, Phys. Rev. B Cond. Matter Mater. Phys. 13 (1976), 5188—5169.

[27] S.L. Dudarev, G.A. Botton, S.Y. Savrasov, C.J. Humphreys, A.P. Sutton, Electron-energy-loss spectra and the structural stability of nickel oxide: an LSDA+U study, Phys. Rev. B Cond. Matter Mater. Phys. 57 (1998) 1505—1509.

[28] V. Anisimov, J. Zaanen, O. Andersen, Band theory and Mott insulators: Hubbard U instead of Stoner, Phys. Rev. B Cond. Matter Mater. Phys. 44 (1991) 943—954.

[29] M. Nolan, S. Grigoleit, D.C. Sayle, S.C. Parker, G.W. Watson, Density functional theory studies of the structure and electronic structure of pure and defective low index surfaces of ceria, Surf. Sci. 576 (2005) 217—229.

[30] M. Nolan, S.C. Parker, G.W. Watson, The electronic structure of oxygen vacancy defects at the low index surfaces of ceria, Surf. Sci. 595 (2005) 223—232.

[31] A. Markovits, M.K. Skalli, C. Minot, G. Pacchioni, N. Lopez, F. Illas, The competition between chemical bonding and magnetism in the adsorption of atomic Ni on MgO(100), J. Chem. Phys. 115 (2001) 8172—8177.

[32] S. Ricote, G. Jacobs, M. Milling, Y. Ji, P.M. Patterson, B.H. Davis, Low temperature water-gas shift: characterization and testing of binary mixed oxides of ceria and zirconia promoted with Pt, Appl. Catal. A Gen. 303 (2006) 35–47.

[33] R. Wang, H. Xu, X. Liu, W. Li, Role of redox couples of $Rh°/Rh^{\delta+}$ and Ce^{4+}/Ce^{3+} in CH_4/CO_2 reforming over $Rh–CeO_2/Al_2O_3$ catalyst, Appl. Catal. A 305 (2006) 204–210.

[34] E. Poggio-Fraccari, B. Irigoyen, G. Baronetti, F. Mariño, Ce–Pr mixed oxides as active supports for water–gas shift reaction: experimental and density functional theory characterization, Appl. Catal. A 485 (2014) 123–132.

[35] Z. Wu, M. Li, J. Howe, H. Mayer, S.H. Overbury, Probing defect sites on CeO_2 nanocrystals with well-defined surface planes by Raman spectroscopy and O_2 adsorption, Langmuir 26 (2010) 16595–16606.

[36] B.M. Reddy, A. Khan, P. Laksmanan, Structural characterization of nanosized $CeO_2–SiO_2$, $CeO_2–TiO_2$, and $CeO_2–ZrO_2$ catalysts by XRD, Raman, and HREM techniques, J. Phys. Chem. B 109 (2005) 3355–3363.

[37] S. Music, A. Saric, S. Popovic, M. Ivanda, Formation and characterisation of nanosize α-Rh_2O_3 particles, J. Mol. Struct. 924 (2009) 221–224.

[38] F. Jin, H. Long, W. Song, G. Xiong, X. Guo, X. Wang, Active phase of a $NiSO_4$ catalyst supported on γ-Al_2O_3 during in situ self-sulfidation for selective hydrodesulfurization, Energy Fuels 27 (2013) 3394–3399.

[39] V. Parvulescu, S. Coman, P. Grange, V.I. Parvulescu, Preparation and characterization of sulfated zirconia catalysts obtained via various procedures, Appl. Catal. A 176 (1999) 27–43.

[40] D. Radwan, L. Saad, S. Mikhail, S.A. Selim, Catalytic evaluation of sulfated zirconia pillared clay in n-hexane transformation, J. Appl. Sci. Res. 5 (2009) 2332–2342.

[41] Q. Pan, L. Qin, J. Liu, H. Wang, Flower-like ZnO–NiO–C films with high reversible capacity and rate capability for lithium-ion batteries, Electrochim. Acta 55 (2010) 5780–5785.

[42] N. Mironova-Ulmane, A. Kuzmin, I. Steins, J. Grabis, I. Sildos, M. Pars, Raman scattering in nanosized nickel oxide NiO, J. Phys. Conf. Ser. 93 (2007) 12039–12044.

[43] R.N. Tarrant, O. Warschkow, D.R. Mc Kenzie, Raman spectra of partially oriented sp^2 carbon films: experimental and modelled, Vib. Spectrosc. 41 (2006) 232–239.

[44] J. Russmann, A. Juan, G. González, B. Irigoyen, Theoretical study of sulfur interactions on $CeO_2(111)$ and $Rh–CeO_2(111)$ surfaces, ACI 2 (3) (2011) 101–110.

[45] Karjalainen, et al., Thermodynamic equilibrium calculations of sulfur poisoning in Ce–O–S and La–O–S systems, Catal. Today 100 (2005) 219–295.